


 Cite this: *Chem. Commun.*, 2021, **57**, 1935

 Received 11th November 2020,
Accepted 12th January 2021

DOI: 10.1039/d0cc07423c

rsc.li/chemcomm

Modulation of charge transport through single-molecule bilactam junctions by tuning hydrogen bonds†

 Yaorong Chen,^{‡a} Hua-Chun Wang,^{‡b} Yongxiang Tang,^{‡a} Yu Zhou,^a Longfeng Huang,^a Jian Cao,^b Chun Tang,^a Manxi Zhang,^a Jia Shi,^a Junyang Liu,^{id a} Xiancheng Ren,^b Yun-Xiang Xu^{id *b} and Wenjing Hong^{id *ac}

Bilactam derivatives with different side groups were synthesized and the twisting angle tuning effect induced by the intramolecular hydrogen bond on the charge transport through their single-molecule junctions was investigated. Molecules with strong intramolecular hydrogen bonds exhibited twice higher conductance because of the reduced dihedral twisting, which was reversible with the addition of hydrogen bond destroying solvent. Our findings reveal that the presence of intramolecular hydrogen bonds promotes the planarization of the molecular structure without additional transmission channels, offering a new strategy for controlling molecular switches via tuning the molecular twisting.

The ultimate goals of molecular electronics are the miniaturization of electronic devices and the integration of functional molecular devices into the circuits.^{1–6} Towards these goals, the functionalization of molecules to construct steerable molecular switches, such as redox,^{7,8} isomerization,^{9,10} bonding formation,^{11,12} gating,¹³ *etc.*, remains a critical step. Previous studies have illustrated that the twisting angle in molecular building blocks effectively changes the intramolecular coupling.^{14,15} An increase of twisting angle between aromatic components leads to a significant decrease in the overlap of π -orbitals, thus resulting in a conductance decrease, which shows a linear relationship between the conductance and the square of the cosine of twisting angle.^{16,17} However, due to the rotation of molecular building blocks and the steric effect,

the electronic structure of molecular junctions is inevitably changed,^{18,19} leaving challenges in controlling molecular switches *via* molecular twisting tuning.

To switch the twisting angle of the single-molecule junction between different states, a simple and direct way is to lock down the rotation of molecular building blocks *via* covalent bonds.^{16,20–22} In this way, the twisting angle between different building blocks could be controlled by the bonding formation to tune the charge transport through molecular devices. However, the lock-down strategy based on non-covalent bonds remains unexplored due to the challenges in the control of intramolecular interaction.²³ Several studies have suggested that intramolecular hydrogen bonds would improve the planarity and conjugation of molecules.^{24–27} The introduction of bilactam units provides a reliable route for forming intramolecular hydrogen bonds, offering new ideas for overcoming the challenges of controlling the twisting between different states.

Herein, we synthesized and investigated the charge transport properties of a series of bilactam derivative molecules with different twisting angles caused by the ring substituents as shown in Fig. 1a. To investigate the influence of the intramolecular interaction on the charge transport, we introduce bilactam units into the rotatable group to form the intramolecular interaction *via* a hydrogen bond to suppresses the freedom of twisting. Combined with the scanning tunneling microscope break junction (STM-BJ) technique and density functional theory (DFT) theoretical calculations, we illustrated that the intramolecular hydrogen bond modulation gives rise to the decrease in the planarity of the molecular structure and a $\sim 200\%$ decrease in molecular conductance. In contrast, similar molecules without hydrogen bonds remain unchanged. Such a robust response behavior during the *in situ* solvent switching cycle provides a promising method to control the charge transport through molecules from a chemical prospect.

To investigate charge transport through these molecules, the single-molecule conductance was measured by the STM-BJ technique in a solution of 1,2,4-trichlorobenzene (TCB) at room

^a State Key Laboratory of Physical Chemistry of Solid Surfaces, iChEM, College of Chemistry and Chemical Engineering, Xiamen University, Xiamen 361005, China. E-mail: whong@xmu.edu.cn

^b College of Polymer Science & Engineering, State Key Laboratory of Polymer Materials Engineering, Sichuan University, Chengdu 610065, China. E-mail: yxxu@scu.edu.cn

^c Beijing National Laboratory for Molecular Sciences, Beijing 100190, China

† Electronic supplementary information (ESI) available: Synthesis steps and characterization data of all compounds; details for single-molecule measurement and theoretical calculations. See DOI: 10.1039/d0cc07423c

‡ These authors contributed equally.

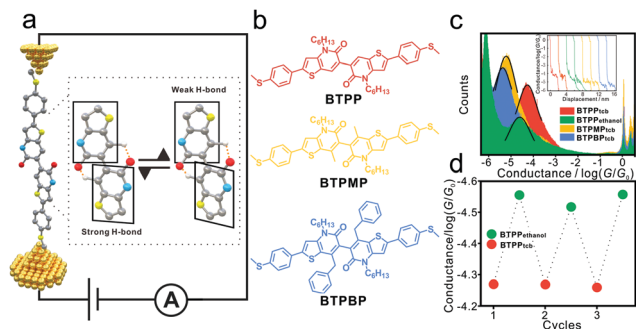


Fig. 1 (a) Schematic of the single-molecule junction and the switching between different states, alkyl chains on N atoms and H atoms except hydrogen bonds are ignored for better demonstration. (b) Molecular structures of **BTTP**, **BTMP** and **BTBP**. (c) The one-dimensional (1D) conductance histogram comparisons of target molecules and typical individual conductance distance traces (inset) of **BTTP_{TCB}**, **BTTP_{ethanol}**, **BTMP_{TCB}** and **BTBP_{TCB}**. (d) Reversible on–off conductance switches of **BTTP** by solvent regulation, the subscript is the solvent.

temperature (more experimental details in the ESI†). Three molecules were employed (Fig. 1b), 4,4′-dihexyl-2,2′-bis(4-(methylthio)phenyl)-[6,6′-bithieno[3,2-*b*]pyridine]-5,5′(4H,4′H)-dione (**BTTP**), 4,4′-dihexyl-7,7′-dimethyl-2,2′-bis(4-(methylthio)phenyl)-[6,6′-bithieno[3,2-*b*]pyridine]-5,5′(4H,4′H)-dione (**BTMP**) and 7,7′-dibenzyl-4,4′-dihexyl-2,2′-bis(4-(methylthio)phenyl)-[6,6′-bithieno[3,2-*b*]pyridine]-5,5′(4H,4′H)-dione (**BTBP**), and the synthetic routes are described in the ESI.†

Typical individual conductance traces are exhibited in the inset of Fig. 1c, where the peak at G_0 (quantum conductance, $G_0 = 2e^2/h$) illustrates the formation of Au–Au atomic point contact.²⁸ The individual conductance plateaus of target molecules are determined to be $10^{-4.24 \pm 0.38} G_0$ (4.46 nS) for **BTTP**, $10^{-4.59 \pm 0.38} G_0$ (1.99 nS) for **BTTP_{ethanol}**, $10^{-5.18 \pm 0.42} G_0$ (0.51 nS) for **BTMP** and $10^{-5.33 \pm 0.33} G_0$ (0.36 nS) for **BTBP**, respectively by Gaussian fitting. The conductance results follow an increasing sequence of **BTBP** < **BTMP** < **BTTP** as the decrease in the twisting angle, and the conductance of **BTTP** is superior to those of **BTMP** and **BTBP** owing to the existence of H-bonds and lack of steric groups. More importantly, after being treated with ethanol, the conductances of **BTMP** and **BTBP** remain unchanged (see Fig. S7, ESI†). While the conductance of the **BTTP** junction was reduced by ~200% without changing the length, indicating that the high conductivity of **BTTP** benefits from the existence of intramolecular hydrogen bonds. Furthermore, after adding ethanol, the solution was vaporized and then pure TCB was added again, the conductance of **BTTP** was reversed back, and remarkably, the cycle by changing the polarity of the solvent can be achieved repeatedly, showing that it is feasible to control the hydrogen bond by solvent to switch the conductance, as shown in Fig. 1d (see more details in the ESI†).

The two-dimensional (2D) conductance and displacement histograms of target molecules are constructed from 3000 stretching traces without data selection. As shown in Fig. 2a–d, the intensity clouds of single-molecule junctions are observed with a similar distance of ~2.3 nm located at ~1.8 nm and

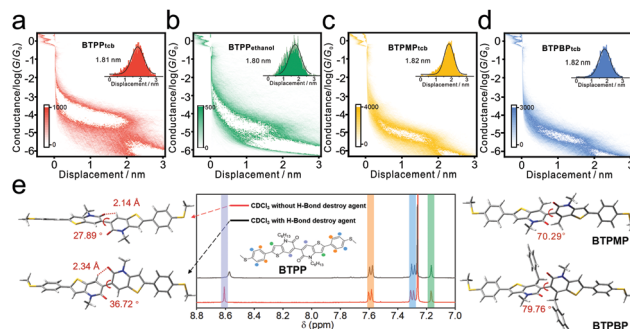


Fig. 2 Two-dimensional (2D) conductance histogram versus relative displacement and relative distance distributions (inset) of **BTTP_{TCB}** (red, a), **BTTP_{ethanol}** (green, b), **BTMP_{TCB}** (yellow, c) and **BTBP_{TCB}** (blue, d). According to the relative distance distributions, the conductance ranges are confirmed to be $10^{-0.3} G_0 \sim 10^{-6.0} G_0$. (e) The optimized molecular structures of **BTTP** before and after mixing with ethanol (left), **BTMP** and **BTBP** (right). And the ^1H NMR of **BTTP** under different solvent (middle).

calibrated with an additional 0.5 nm Au–Au snap-back distance.²⁹ Since the lengths of single-molecule junctions are comparable to a fully stretched configuration bridge between two electrodes, the variation in conductance originates from the different twisting angle between two building blocks of single-molecule junctions. To better understand the difference in twisting structures, the optimization structures of **BTTP**, **BTMP** and **BTBP** were obtained by Gaussian software, as shown in Fig. 2e. The dihedral angle of the building blocks follows a sequence of **BTTP** (27.89°) < **BTMP** (70.29°) < **BTBP** (79.76°).

Notably, for **BTTP**, the length of O–H (~2.14 Å) indicates the formation of hydrogen bonds, which corresponds to the lowest potential energy structure in Fig. S10 (ESI†).^{30–32} For comparison, the dihedral of **BTTP** mixed with ethanol is 36.72°, which is comparable to the degree of the corresponding crystalline characterized by X-ray diffraction.³³ The displacement (from δ 8.60 to δ 8.57, Fig. 2e) in ^1H NMR indicates that the hydrogen bonds are broken by introducing a hydrogen bond destroying agent, and therefore the smaller dihedral angle of **BTTP** is due to the confinement of intramolecular hydrogen bonds and bare steric hindrance. In contrast, the intramolecular hydrogen bonds of **BTMP** and **BTBP** are unable to form (see Fig. S2–S4, ESI†) due to large steric hindrance, and thus there is no change in conductance after introducing ethanol. Furthermore, the minor dihedral angle difference between **BTMP** and **BTBP** indicates that the increase of the steric-hindrance of the ring substitution weakly promotes the further increase of dihedral angle.

To further investigate the intramolecular coupling, flicker noise measurements were performed.³⁴ According to the above-mentioned results, the molecular junction elongation was paused for 150 ms to extract the conductance signals within the period for flicker noise analysis (the typical traces are shown in Fig. 3a, see the ESI,† for more details).³⁵ Due to the volatilization of ethanol, the flicker noise of **BTTP_{ethanol}** is inevitably affected. Therefore, we only discuss the situation with pure TCB solvent. We found that the scale of the noise power of **BTTP** is $G^{1.4}$ due to the not fully planar conjugated configuration (Fig. 3b), indicating that the charge transport

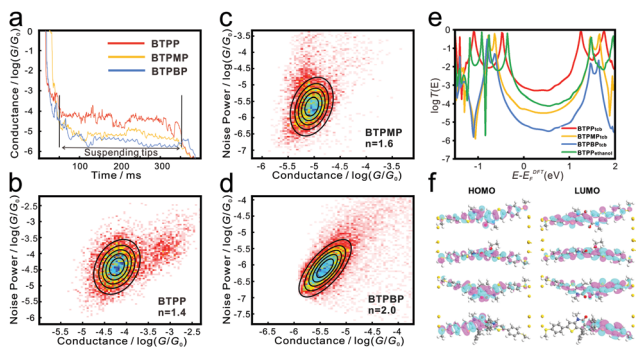


Fig. 3 (a) The typical hover conductance traces of target molecules. The noise power versus averaged conductance for (b) **BTTP**, (c) **BTMP** and (d) **BTBP**. (e) DFT calculations of transmission analysis. The calculation transmission function of **BTTP_{tcb}** (red), **BTTP_{ethanol}** (green), **BTMP_{tcb}** (yellow) and **BTBP_{tcb}** (blue) versus E_F (eV). (f) The spatial distribution of orbital levels of **BTTP_{tcb}**, **BTTP_{ethanol}**, **BTMP_{tcb}** and **BTBP_{tcb}** (from up to down) related to the Fermi energy with an isovalue of 0.05.

through **BTTP** is primarily dominated by through-bond coupling and partially through-space coupling. In contrast, for **BTMP**, the noise power of $G^{1.6}$ (Fig. 3c) indicates the presence of primary through-space coupling and partial through-bond coupling. While for **BTBP**, the noise power scales as $G^{2.0}$ (Fig. 3d), which indicates that the through-space coupling is dominant. Notably, the decrease in conductance of these molecular junctions is associated with an increase in the predominant proportion of through-space coupling, suggesting that the increase of twisting angle promotes the transformation of charge transport through the molecular junction from through-bond to through-space.

To further understand the role of the hydrogen bond on the intramolecular coupling, the transmission spectra of the single-molecule junctions at zero bias were carried out.^{36,37} The results were obtained in DFT with the non-equilibrium Green's function (NEGF) method by using the Quantum ATK software package shown in Fig. 3e (more details in the ESI†). The intramolecular hydrogen bond in **BTTP** diminishes the dihedral angle of the centre molecular blocks, which reduced the twisting of the molecule, thus improving the conduction through the π system. More interestingly, the absolute value of the HOMO (highest occupied molecular orbital, -0.48 eV) and the LUMO (lowest unoccupied molecular orbital, 1.24 eV) of **BTTP** is smaller than that of **BTBP** (HOMO of -0.64 eV and LUMO of 1.46 eV). We found that the twisting angles of the molecule do not change the dominated transmission energy level but only broaden the HOMO–LUMO gap confirmed by the UV-Vis spectrum (Fig. S1, ESI†), which is also accompanied by a significant difference in the transmission near the Fermi energy as shown in Fig. 3e. More importantly, compared with the independently distributed energy levels of the planar configuration, the HOMO and HOMO–1 (or LUMO and LUMO+1) energy levels are quasi-degenerate in the orthogonal configuration.³⁸ Since the energy levels of target molecules tend to be quasi-degenerate as the increase in twisting angle, the superposition of two degenerate orbitals with an opposite

symmetry leads to non-completely destructive quantum interference, and thus the transmission is obviously inhibited.

To further reveal this phenomenon from the perspective of molecular orbitals, Molecular Projected Self-consistent Hamiltonian (MPSH) analysis using the junction configuration were all employed to plot the energies and spatial distribution of the frontier orbitals (more details in Fig. S12, ESI†).^{18,39} The order of HOMO–LUMO gap is in accordance with the above conductance measurement results (**BTTP_{tcb}** < **BTTP_{ethanol}** < **BTMP_{tcb}** < **BTBP_{tcb}**). That is, a larger gap is generally associated with a low conductance of molecular junction. As shown in Fig. 3f, the electronic structures of target molecules tend to be localized as the dihedral angle increases. The separation of the frontier molecular orbitals is ascribed to the weak coupling of building blocks caused by the orthogonality of the π -orbitals onto the two connected rings, which suppresses the charge transport through the bond, making the transport through space become dominated and leading to lower conductance of the molecular junction. The through-space conjugation between the oxygen atom and the hydrogen atom does not appear in the frontier orbitals, indicating that the intramolecular H-bond does not act as an additional conduction channel for this twisting structure but it only limits the twisting angles. Our experimental and theoretical results manifest that the dihedral angle between the molecular building blocks can be adjusted by intramolecular interactions, providing an effective chemical control strategy.

In conclusion, we investigated the charge transport through bilactam derivatives with different dihedral angles using the STM-BJ technique. Our results demonstrate the control of the intramolecular hydrogen bond, which results in a dihedral change of 8.83° , could elaborately tune the charge transport through the molecules, and the conductance switching could be reversibly achieved for cycling. Combined with theoretical calculations, the localization of the electronic structure originated from the twisting structure which hinders charge transport, resulting in the transition from through-bond transmission to through-space transmission, as revealed by the flicker noise analysis. In comparison, the presence of intramolecular hydrogen bonds does not provide a conductive channel but brings a change in the twisting between molecular building blocks. Our findings provide a strategy for the design of reversible molecular switches to manipulate charge transport through the single-molecule junction *via* the control of coupling between different molecular building blocks.

This work was supported by the Natural Science Foundation of China (No. 21673195, 21722305, 21703188, 21933012, 31871877, U1705254, and 51403135), the National Key R&D Program of China (2017YFA0204902), Sichuan Science and Technology Program (Grant No. 2019YJ0123), Fundamental Research Funds for the Central Universities (No. 20720200068), and State Key Laboratory of Polymer Materials Engineering (Grant No. sklpmc 2014-3-16).

Conflicts of interest

There are no conflicts to declare.

Notes and references

- M. Ratner, *Nat. Nanotechnol.*, 2013, **8**, 378–381.
- E. Lortscher, *Nat. Nanotechnol.*, 2013, **8**, 381–384.
- L. Chen, A. Feng, M. Wang, J. Liu, W. Hong, X. Guo and D. Xiang, *Sci. China: Chem.*, 2018, **61**, 1368–1384.
- D. Xiang, X. Wang, C. Jia, T. Lee and X. Guo, *Chem. Rev.*, 2016, **116**, 4318–4440.
- S. H. Choi, B. Kim and C. D. Frisbie, *Science*, 2008, **320**, 1482–1486.
- S. J. van der Molen, R. Naaman, E. Scheer, J. B. Neaton, A. Nitzan, D. Natelson, N. J. Tao, H. van der Zant, M. Mayor, M. Ruben, M. Reed and M. Calame, *Nat. Nanotechnol.*, 2013, **8**, 385–389.
- F. Chen, J. He, C. Nuckolls, T. Roberts, J. E. Klare and S. Lindsay, *Nano Lett.*, 2005, **5**, 503–506.
- L. J. O'Driscoll, J. M. Hamill, I. Grace, B. W. Nielsen, E. Almutib, Y. C. Fu, W. J. Hong, C. J. Lambert and J. O. Jeppesen, *Chem. Sci.*, 2017, **8**, 6123–6130.
- E. Leary, C. Roche, H. W. Jiang, I. Grace, M. T. Gonzalez, G. Rubio-Bollinger, C. Romero-Muniz, Y. Y. Xiong, Q. Al-Galiby, M. Noori, M. A. Lebedeva, K. Porfyrakis, N. Agrait, A. Hodgson, S. J. Higgins, C. J. Lambert, H. L. Anderson and R. J. Nichols, *J. Am. Chem. Soc.*, 2018, **140**, 710–718.
- X. D. Yin, J. Z. Low, K. J. Fallon, D. W. Paley and L. M. Campos, *Chem. Sci.*, 2019, **10**, 10733–10739.
- T. Sandler, K. Luka-Guth, M. Wieser, Lokamani, J. Wolf, M. Helm, S. Gemming, J. Kerbusch, E. Scheer, T. Huhn and A. Erbe, *Adv. Sci.*, 2015, **2**, 1500017.
- M. S. Inkpen, Y. R. Leroux, P. Hapiot, L. M. Campos and L. Venkataraman, *Chem. Sci.*, 2017, **8**, 4340–4346.
- L. Yuan, L. J. Wang, A. R. Garrigues, L. Jiang, H. V. Annadata, M. A. Antonana, E. Barco and C. A. Nijhuis, *Nat. Nanotechnol.*, 2018, **13**, 322–329.
- C. Jia and X. Guo, *Chem. Soc. Rev.*, 2013, **42**, 5642–5660.
- F. B. Meng, Y. M. Hervault, Q. Shao, B. H. Hu, L. Norel, S. Rigaut and X. D. Chen, *Nat. Commun.*, 2014, **5**, 3023.
- L. Venkataraman, J. E. Klare, C. Nuckolls, M. S. Hybertsen and M. L. Steigerwald, *Nature*, 2006, **442**, 904–907.
- C. M. Finch, S. Sirichantaropass, S. W. Bailey, I. M. Grace, V. M. Garcia-Suarez and C. J. Lambert, *J. Phys.: Condens. Matter*, 2008, **20**, 022203.
- Z. Chen, L. Chen, J. Liu, R. Li, C. Tang, Y. Hua, L. Chen, J. Shi, Y. Yang, J. Liu, J. Zheng, L. Chen, J. Cao, H. Chen, H. Xia and W. Hong, *J. Phys. Chem. Lett.*, 2019, **10**, 3453–3458.
- M. Kiguchi, S. Nakashima, T. Tada, S. Watanabe, S. Tsuda, Y. Tsuji and J. Terao, *Small*, 2012, **8**, 726–730.
- E. J. Dell, B. Capozzi, K. H. DuBay, T. C. Berkelbach, J. R. Moreno, D. R. Reichman, L. Venkataraman and L. M. Campos, *J. Am. Chem. Soc.*, 2013, **135**, 11724–11727.
- A. Mishchenko, D. Vonlanthen, V. Meded, M. Burkle, C. Li, I. V. Pobelov, A. Bagrets, J. K. Viljas, F. Pauly, F. Evers, M. Mayor and T. Wandlowski, *Nano Lett.*, 2010, **10**, 156–163.
- S. Soni, G. Ye, J. Zheng, Y. X. Zhang, A. Asyuda, M. Zharnikov, W. Hong and R. C. Chiechi, *Angew. Chem., Int. Ed.*, 2020, **59**, 14308–14312.
- Y. C. Li, B. H. Xiao, R. S. Chen, H. J. Chen, J. Q. Dong, Y. C. Liu and S. Chang, *Chem. Commun.*, 2019, **55**, 8325–8328.
- W. Hu, N. B. Zhu, W. Tang and D. H. Zhao, *Org. Lett.*, 2008, **10**, 2669–2672.
- Y. Song, Z. Xie, M. Z. Wei, J. C. Leng, Z. L. Li and C. K. Wang, *Comput. Mater. Sci.*, 2015, **108**, 8–13.
- L. T. Dou, W. H. Chang, J. Gao, C. C. Chen, J. B. You and Y. Yang, *Adv. Mater.*, 2013, **25**, 825–831.
- D. Nunez-Villanueva and C. A. Hunter, *Chem. Sci.*, 2017, **8**, 206–213.
- W. Hong, D. Z. Manrique, P. Moreno-Garcia, M. Gulcur, A. Mishchenko, C. J. Lambert, M. R. Bryce and T. Wandlowski, *J. Am. Chem. Soc.*, 2012, **134**, 2292–2304.
- C. Tang, J. Zheng, Y. Ye, J. Liu, L. Chen, Z. Yan, Z. Chen, L. Chen, X. Huang, J. Bai, Z. Chen, J. Shi, H. Xia and W. Hong, *iScience*, 2020, **23**, 100770.
- C. Y. Fu, P. J. Beldon and D. F. Perepichka, *Chem. Mater.*, 2017, **29**, 2979–2987.
- A. Shukla, E. Khan, A. Srivastava, P. Tandon and K. Sinha, *Mol. Simul.*, 2016, **42**, 863–873.
- J. Sandoval-Lira, L. Fuentes, L. Quintero, H. Hopfl, J. M. Hernandez-Perez, J. L. Teran and F. Sartillo-Piscil, *J. Org. Chem.*, 2015, **80**, 4481–4490.
- H. C. Wang, M. R. Ren, J. Cao, H. B. Yin, G. C. Zhang, J. Y. Xiao, X. C. Ren, L. Yip and Y. X. Xu, *J. Mater. Chem. C*, 2019, **7**, 12290–12296.
- O. Adak, E. Rosenthal, J. Meisner, E. F. Andrade, A. N. Pasupathy, C. Nuckolls, M. S. Hybertsen and L. Venkataraman, *Nano Lett.*, 2015, **15**, 4143–4149.
- C. Tang, L. Chen, L. Zhang, Z. Chen, G. Li, Z. Yan, L. Lin, J. Liu, L. Huang, Y. Ye, Y. Hua, J. Shi, H. Xia and W. Hong, *Angew. Chem., Int. Ed.*, 2019, **58**, 10601–10605.
- B. Capozzi, J. L. Xia, O. Adak, E. J. Dell, Z. F. Liu, J. C. Taylor, J. B. Neaton, L. M. Campos and L. Venkataraman, *Nat. Nanotechnol.*, 2015, **10**, 522–527.
- M. Brandbyge, J. L. Mozos, P. Ordejon, J. Taylor and K. Stokbro, *Phys. Rev. B: Condens. Matter Mater. Phys.*, 2002, **65**, 165401.
- T. Markussen and K. S. Thygesen, *Phys. Rev. B: Condens. Matter Mater. Phys.*, 2014, **89**, 085420.
- K. Stokbro, J. Taylor, M. Brandbyge, J. L. Mozos and P. Ordejon, *Comput. Mater. Sci.*, 2003, **27**, 151–160.